Volatile Organic Compound Detection Using Insect Odorant-Receptor Functionalised Field-Effect Transistors

by

Eddyn Oswald Perkins Treacher

A thesis submitted in fulfilment of the
requirements of the degree of
Doctor of Philosophy in Physics
School of Physical and Chemical Sciences
Te Herenga Waka - Victoria University of Wellington

May 2024

Table of contents

Acknowledgements

69450

Rifat, Alex - vapour sensor Erica Cassie - FET sensing setup Rob Keyzers and Jennie Ramirez-Garcia - NMR spectra Patricia Hunt - Computational chemistry

1. Carbon Nanotube and Graphene Field-Effect Transistors

1.1. Introduction

Out of a wide range of available transducer options available for the creation of compact, portable and highly-integrated biosensors, field-effect transistors are among the most promising. Field-effect transistors consist of two conductive electrodes on either side of a semiconducting channel, with the higher potential electrode called the source electrode and lower potential electrode called the drain electrode, alongside an isolated gate electrode. An applied electric field from the gate electrode capacitively controls channel resistance, giving rise to the label 'field-effect'. By adjusting gate voltage, channel current can be varied over several orders of magnitude. The ability of this simple structure to obtain a large signal response from small changes in channel behaviour is highly advantageous for sensor applications [1], [2]. Field-effect transistors are unipolar transistors; channel conduction either mainly consists of electron carriers, which is called n-type conduction, or hole carriers, which is called p-type conduction [2].

Carbon nanotube network and graphene field-effect transistors (CNTFETs and GFETs) are both examples of a class of field-effect transistors called thin-film transistors (TFTs). These transistors are closely related to the commonly-used metal oxide semiconductor field-effect transistor (MOSFET). Unlike MOSFETs, thin-film transistors do not use the substrate as the channel. Instead, current passes through a semiconducting film on the surface of the device. Since only a thin film is required for the channel, an important advantage of thin-film transistors over MOSFETs is their ability to use a range of flexible and stretchable substrates that may not be conductive. A wide variety of semiconducting films may be used; the films discussed here are carbon nanotube networks and graphene, which both fall under the class of carbon-based 2D nanomaterials. [1], [3].

1.2. Thin-Film Field-Effect Transistors

1.2.1. Structure and Gating

The basic components of the thin-film transistor can be configured in a variety of different ways. These configurations include the back-gated field-effect transistor and the

liquid-gated transistor, also known as the electrolyte-gated transistor. The relatively simple back-gated configuration, shown in Figure 1.1 (a), uses the silicon substrate as the gate. The channel is isolated from the gate with a thin silicon dioxide layer. The device characteristics are determined by the gate capacitance, which is made up of the capacitance of the oxide layer (C_{ox}) and the quantum capacitance [4] of the 2D nanomaterial (C_{qm}). A liquid-gated device, shown in Figure 1.1 (b), gives rise to enhanced device sensitivity in an aqueous environment. In this configuration, a reference electrode is used as the gate, with the channel isolated from the gate by an electrolyte solution. This solution can be polymer, gel or water-based. The gate capacitance is a series combination of the electrical double layer capacitance of the electrolyte (C_{edl}), at both the channel-liquid and liquid-electrode interfaces, and C_{qm} [1], [5].

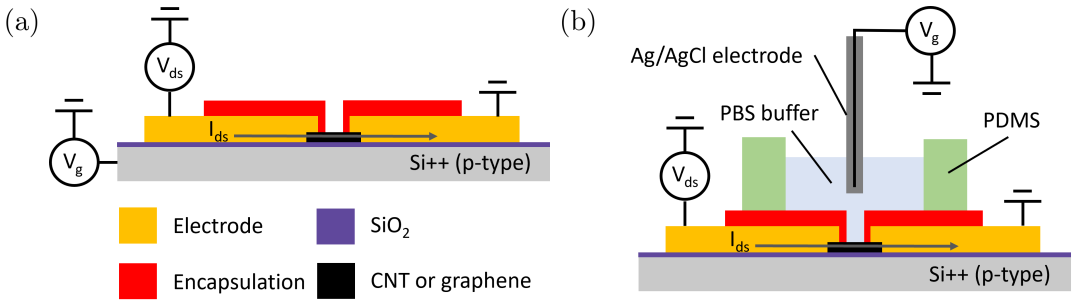

Figure 1.1.: Schematics (not to scale) showing the side-view cross-section of a thin-film field-effect transistor in both the (a) back-gated and (b) liquid-gated configuration. A graphene monolayer or a carbon nanotube network is used as the transistor thin-film.

The type of structure used determines the type of sensing mechanisms available, which can include electrostatic gating, Schottky barrier modulation, capacitance modulation or charge scattering [6].

discuss Debye length in the context of gating!!! mention plasma lol

1.2.2. Electrical Characterisation

CNTFETs are traditionally *p*-type transistors with positive charge carriers [7], [8], while GFETs are ambipolar [9]. Applying an gate voltage V_g to the gate of a CNTFET or GFET increases, or decreases, the number of available charge carriers, by bringing the relevant charge-carrying band closer to, or further away from, the Fermi level of the channel [10]. An example of both back-gated and liquid-gated transfer characteristics from thin-film transistors are shown in Figure 1.3.

V_{ds} is the voltage between the source and drain electrodes at either end of the semiconducting channel, and is known as the 'drain bias'. V_g is the potential beneath the gate, and is known as the 'gate bias'. The gate is insulated from the semiconducting

channel by an oxide layer. I_d is the current that flows through the FET from the source to the drain. The current-voltage plot of I_d against V_g is called the 'transfer characteristic curve' of the FET, while the I-V curve of I_d against V_{ds} is called the 'source-drain characteristic curve' of the FET.

V_g is used to turn the FET on or off. A FET is known as 'normally-off' if at zero gate bias the channel conductance is very low, and gate voltage must be applied to make the channel conductive. Conversely, a FET is 'normally-on' when the channel is conductive with zero gate bias and must have a gate voltage applied to be turned off. For p-type channel FETs, negative Vg brings the valence band closer to the Fermi level, meaning more positive charge carriers are available. Therefore these devices are made more conductive with a more negative gate bias; an increase in V_g reduces I_d. The opposite is true for n-type channel devices, where a more positive V_g brings the conduction band closer to the Fermi level, meaning more negative charge carriers are available, making the device more conductive. The increased availability of majority carriers in both cases is known as 'accumulation'. Figure 1.2 illustrates accumulation in each situation.

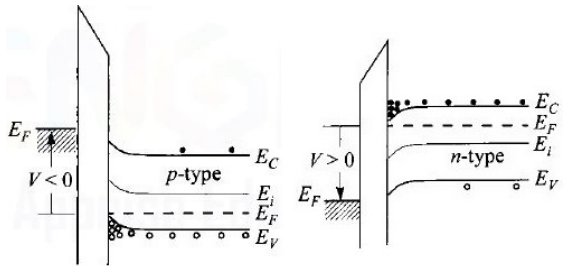

Figure 1.2.: Energy band diagrams for a FET device under accumulation conditions, where the left side of each diagram is the gate region, while the right side is the channel region [10].

An important attribute of the transfer characteristic curve for all thin-film FETs is the on-off current ratio. On-off current ratio is the ratio of the current through a device when gated fully "off" with a positive voltage, to the current through the device when gated fully "on" with a negative voltage [11]. The off current in an ambipolar FET can be defined as the minimum current during the transfer sweep, where the majority carrier transitions from being holes to electrons or vice versa. For example, the on current of the channel shown in Figure 1.3 (b) is 741.5 nA, the off current is 0.2 nA, and therefore the on-off ratio is ~ 3000. In contrast, even when 10 V is applied, the backgated device shown in Figure 1.3 (a) is never gated fully off. Application of higher voltages to the gate result in significant leakage currents through the gate, and can even result in irreversible breakdown of the oxide layer [10]. Being able to traverse both on and off regimes over a limited voltage interval is one of the many advantages of the liquid-gated configuration.

In the linear I_d-V_{ds} regime, transconductance is given by dI_d/dV_g, which gives a measure of the mobility of the charge carriers in the device channel [7], [10], [11].

Traditionally, for sensor applications V_g is chosen to maximise transconductance, as this is considered to be the operating point where the channel is most sensitive to changes in the local environment [9], [12]. However, for carbon nanotube FETs it has been suggested that operating in the subthreshold regime gives improved signal-to-noise ratio [13]. A discussion about the subthreshold regime of CNTFETs is found in Section 1.4.3.

subthreshold regime Previous biosensor research

A FET contains a potential barrier acting against charge carriers at the junctions between the channel and the contacts, known as 'Schottky barriers'. These barriers arise because of the Fermi energy difference between the metal contacts and the semiconducting channel, and are characterised by the size of the barrier potential φ_B [14]. Increased barrier size leads to increased resistance between the component materials of the FET [15].

As $C_{qm} \gg C_{edl}$, hysteresis is significantly reduced for the liquid-gated configuration relative to the back-gated configuration. In this work, the liquid-gate is completely isolated from the channel, which ensures sensing is not due to modulation of the Schottky barrier between the channel and electrodes, but this is not always true for thin-film transistors in the literature [5].

Channel carriers in a FET can be accelerated by a sufficiently high gate-channel field into surmounting the insulating barrier between the gate and channel. This is known as 'breakdown'. The breakdown voltage V_b gives an upper limit to the bias able to be applied across the device without the device being destroyed. Percolation theory can be used to explain breakdown. As energetic carriers pass through the oxide, defects are created randomly. When these random defects are dense enough to form a chain from the gate to the semiconductor, a short is created and breakdown occurs. With decreased oxide thickness the the required voltage for breakdown also decreases, due to increased carrier tunnelling.

1.2.3. Current Sampling

It is important to account for the changes in current that occur during a sensing run that are unrelated to sensing, and try to minimise these changes as much as possible. These changes are due to a variety of causes and can be categorised as various types of noise and baseline drift. (1/f noise paper, heller paper)

1.3. Graphene Field-Effect Transistors

1.3.1. Electrical Characterisation

As graphene FETs are ambipolar, they do not possess a characteristic 'off' regime. In normal operation of a GFET, the lowest voltage obtainable by gating is known as the

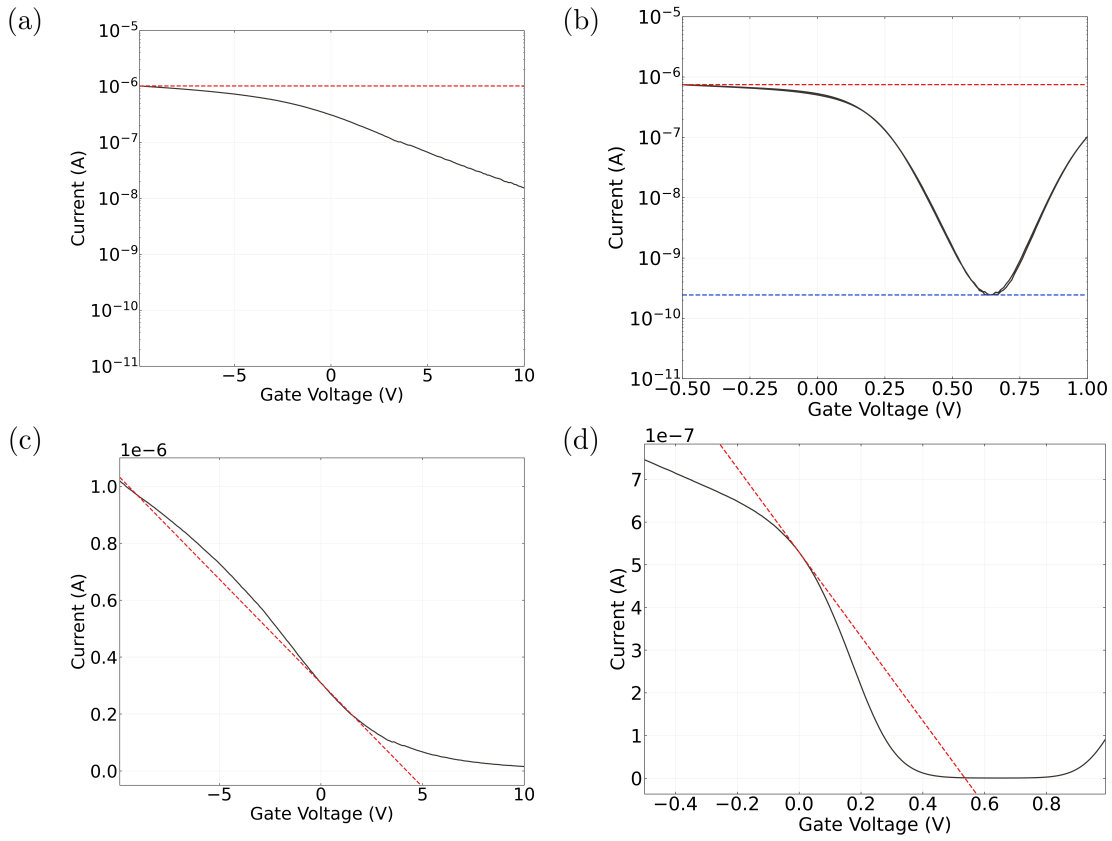

Figure 1.3.: Examples of field-effect transistor transfer characteristics taken at V_{ds} = 100 mV from two different device channels. A logarithmic scale is used in (a) and (b), while a linear scale is used in (c) and (d). The device channel in (a) and (c) was backgated while the device channel in (b) and (d) was liquid-gated. The "on" current in (a) and (b) is shown with a red horizontal line, while the "off" current in (b) is shown with a blue horizontal line. The linear fit with gradient corresponding to transconductance at $V_g = 0$ V is shown in (c) and (d) with a dotted red line.

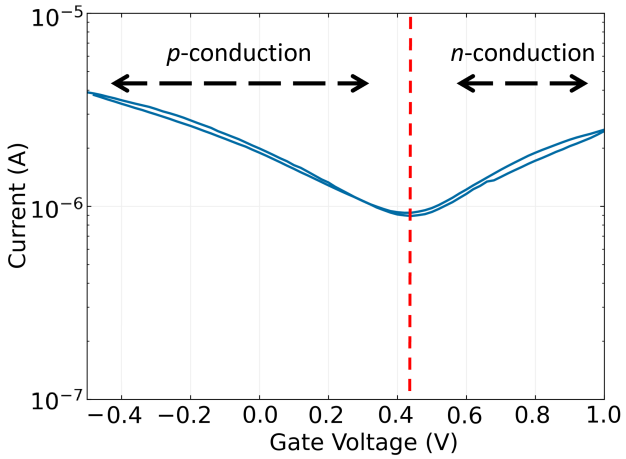

Figure 1.4.: Transfer characteristics of a graphene field-effect transistor channel showing the regions of hole conduction and electron conduction. The red dotted line indicates the Dirac point voltage of the device channel.

Dirac voltage [16].

Quantative measurement of leftward shift in transfer curve Use minima of curve in reverse sweep direction (more consistent than reading in forward sweep direction) I compared the transfer characteristics after then rinse steps to the pristine characteristics Transfer shifts where current drops to zero are excluded (indicates delamination/damage to channel)

1.4. Random-Network Carbon Nanotube Field-Effect Transistors

1.4.1. Composition and Chirality

A single-walled carbon nanotube (SWCNT) consists of a graphene sheet, a flat carbon lattice with hexagonal cells, rolled up into a cylinder. Since their discovery in 1991, a wide range of device applications for carbon nanotubes (CNTs) have been proposed, based on CNTs being highly sensitive to their environment [14], [17]–[19]. This high sensitivity is due to the high surface-to-volume ratio of the CNTs, which maximises the exposure of this electrically sensitive structure to its surroundings [1], [2]. SWCNT-based devices consume little power, operate quickly and are highly flexible [1], [19]. Nanotubes in a network can have semiconducting characteristics (s-CNTs) or metallic characteristics (m-CNTs), depending on their chirality [7], [8]. A single CNT will therefore have different properties than a network of CNTs, where the individual electrical properties of the CNT tubes are averaged out across the network [17]. The contact between the electrodes

and carbon nanotubes determines the behaviour of channel carriers. The properties of electrodes generally used in CNT FETs means they usually operate as p-type transistors [2].

Semiconducting carbon nanotubes have particular advantages for use in sensor applications, including a high carrier mobility, compatibility with many biological targets, and ease of processing [1].

1.4.2. Network Morphology

1.4.3. Electrical Characterisation

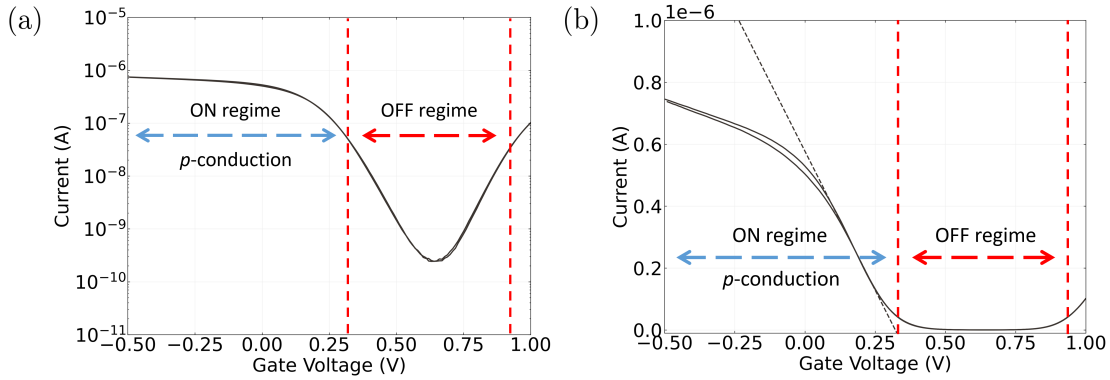

Figure 1.5.: Transfer characteristics of a single carbon nanotube network field-effect transistor channel, using a logarithmic scale in (a) and using a linear scale in (b) to emphasise different features of the same dataset. The subthreshold slope is shown with a black dotted line, while the threshold voltages are shown with red dotted lines. The ON and OFF regimes are also indicated on both figures.

Threshold Voltage

The threshold voltage is the voltage required to fully deplete the device channel of charge carriers [7]. It can be estimated by extrapolating the linear part of the transfer characteristics of a device to the V_g axis.

The FET turns on at the 'threshold voltage', $V_g = V_t$. For the p-type FET, when $V_g > V_t$, I_d increases linearly.

After decreasing past V_t, I_d stays constant at its 'on' value I_{ON}. The ratio of I_{ON} to the I_{OFF} current is known as the FET device's 'on-off ratio', I_{ON}/I_{OFF}. The threshold voltage can be calculated by using an FET's transfer characteristics. From extrapolating

the trendline of the linear region to the V_g axis, the intercept V_{gInt} is approximately equivalent to V_t [10].

Threshold Voltage: minimum gate-to-source voltage that is needed to create a conducting path between the electrodes

Quantative measurement of leftward shift in transfer curve Use minima of curve in reverse sweep direction (more consistent than reading in forward sweep direction) I compared the transfer characteristics after then rinse steps to the pristine characteristics Transfer shifts where current drops to zero are excluded (indicates delamination/damage to channel)

Second quantative measurement of leftward shift in transfer curve Use curve in reverse sweep direction (more consistent than reading in forward sweep direction) Separate readings for left and right hand sides of transfer curve (left side = electrons dominant carrier, right side = holes dominant carrier) Transfer shifts where current drops to zero are excluded (indicates delamination/damage to channel) This gives us a quantitative idea of whether the transfer shifts in slides 5/6 are stable (remain the same/similar after rinse steps)

A. Vapour System Hardware

Table A.1.: Major components used in construction of the vapour delivery system described in this thesis.

Description	Part No.	Manufacturer
Mass flow controller, 20 sccm full scale	GE50A013201SBV020	MKS Instruments
Mass flow controller, 200 sccm full scale	GE50A013202SBV020	MKS Instruments
Mass flow controller, 500 sccm full scale	FC-2901V	Tylan
Analogue flowmeter, 240 sccm max. flow	116261-30	Dwyer
Micro diaphragm pump	P200-B3C5V-35000	Xavitech
Analogue flow controller, for micro diaphragm pump	X3000450	Xavitech
10 mL Schott bottle	218010802	Duran
PTFE connection cap system	Z742273	Duran
Baseline VOC-TRAQ flow cell, red	043-951	Mocon
Humidity and temperature sensor	T9602	Telaire
Enclosure, for humidity and temperature sensor	MC001189	Multicomp Pro

B. Python Code for Data Analysis

B.1. Code Repository

The code used for general analysis of field-effect transistor devices in this thesis was written with Python 3.8.8. Contributors to the code used include Erica Cassie, Erica Happe, Marissa Dierkes and Leo Browning. The code is located on GitHub and the research group OneDrive, and is available on request.

B.2. Atomic Force Microscope Histogram Analysis

The purpose of this code is to analyse atomic force microscope (AFM) images of carbon nanotube networks in .xyz format taken using an atomic force microscope and processed in Gwyddion (see **?@sec-afm-characterisation**). It was originally designed by Erica Happe in Matlab, and adapted by Marissa Dierkes and myself for use in Python. The code imports the .xyz data and sorts it into bins 0.15 nm in size for processing. To perform skew-normal distribution fits, both *scipy.optimize.curve_fit* and *scipy.stats.skewnorm* modules are used in this code.

B.3. Raman Spectroscopy Analysis

The purpose of this code is to analyse a series of Raman spectra taken at different points on a single film (see **?@sec-raman-characterisation**). Data is imported in a series of tab-delimited text files, with the low wavenumber spectrum ($100\ \mathrm{cm}^{-1} - 650\ \mathrm{cm}^{-1}$) and high wavenumber spectrum ($1300\ \mathrm{cm}^{-1} - 1650\ \mathrm{cm}^{-1}$) imported in separate datafiles for each scan location.

B.4. Field-Effect Transistor Analysis

The purpose of this code is to analyse electrical measurements taken of field-effect transistor (FET) devices. Electrical measurements were either taken from the Keysight 4156C Semiconductor Parameter Analyser, National Instruments NI-PXIe or Keysight B1500A Semiconductor Device Analyser as discussed in **?@sec-electrical-characterisation**;

the code is able to analyse data in .csv format taken from all three measurement setups. The main Python file in the code base consists of three related but independent modules: the first analyses and plots sensing data from the FET devices, the second analyses and plots transfer characteristics from channels across a device, and the third compares individual channel characteristics before and after a modification or after each of several modifications. The code base also features a separate config file and style sheet which govern the behaviour of the main code. The code base was designed collaboratively by myself and Erica Cassie over GitHub using the Sourcetree Git GUI.

Bibliography

[1] Bajramshahe Shkodra, Mattia Petrelli, Martina Aurora Costa Angeli, et al. "Electrolyte-gated carbon nanotube field-effect transistor-based biosensors: Principles and applications". In: *Applied Physics Reviews* 8.4 (Dec. 2021), p. 41325. ISSN: 19319401. DOI: 10.1063/5.0058591/1076095. URL: /aip/apr/article/8/4/041325/1076095/Electrolyte-gated-carbon-nanotube-field-effect.

[2] Xuesong Yao, Yalei Zhang, Wanlin Jin, et al. "Carbon Nanotube Field-Effect Transistor-Based Chemical and Biological Sensors". In: *Sensors 2021, Vol. 21, Page 995* 21.3 (Feb. 2021), p. 995. ISSN: 1424-8220. DOI: 10.3390/S21030995. URL: https://www.mdpi.com/1424-8220/21/3/995/htm%20https://www.mdpi.com/1424-8220/21/3/995.

[3] Dong Ming Sun, Chang Liu, Wen Cai Ren, et al. "A Review of Carbon Nanotube- and Graphene-Based Flexible Thin-Film Transistors". In: *Small* 9.8 (Apr. 2013), pp. 1188–1205. ISSN: 1613-6829. DOI: 10.1002/SMLL.201203154. URL: https://onlinelibrary.wiley.com/doi/full/10.1002/smll.201203154%20https://onlinelibrary.wiley.com/doi/abs/10.1002/smll.201203154%20https://onlinelibrary.wiley.com/doi/10.1002/smll.201203154.

[4] Jilin Xia, Fang Chen, Jinghong Li, et al. "Measurement of the quantum capacitance of graphene". In: *Nature Nanotechnology 2009 4:8* 4.8 (July 2009), pp. 505–509. ISSN: 1748-3395. DOI: 10.1038/nnano.2009.177. URL: https://www.nature.com/articles/nnano.2009.177.

[5] Zhongyu Li, Mengmeng Xiao, Chuanhong Jin, et al. "Toward the Commercialization of Carbon Nanotube Field Effect Transistor Biosensors". In: *Biosensors 2023, Vol. 13, Page 326* 13.3 (Feb. 2023), p. 326. ISSN: 2079-6374. DOI: 10.3390/BIOS13030326. URL: https://www.mdpi.com/2079-6374/13/3/326/htm%20https://www.mdpi.com/2079-6374/13/3/326.

[6] Iddo Heller, Anne M. Janssens, Jaan Männik, et al. "Identifying the mechanism of biosensing with carbon nanotube transistors". In: *Nano Letters* 8.2 (Feb. 2008), pp. 591–595. ISSN: 15306984. DOI: 10.1021/NL072996I. URL: https://pubs.acs.org/doi/full/10.1021/nl072996i.

[7] R. Martel, T. Schmidt, H. R. Shea, et al. "Single- and multi-wall carbon nanotube field-effect transistors". In: *Applied Physics Letters* 73.17 (Oct. 1998), pp. 2447–2449. ISSN: 0003-6951. DOI: 10.1063/1.122477. URL: /aip/apl/article/73/17/2447/1023171/Single-and-multi-wall-carbon-nanotube-field-effect.

[8] Jing Kong, Nathan R. Franklin, Chongwu Zhou, et al. "Nanotube molecular wires as chemical sensors". In: *Science (New York, N.Y.)* 287.5453 (Jan. 2000), pp. 622–625. ISSN: 1095-9203. DOI: 10.1126/SCIENCE.287.5453.622. URL: https://pubmed.ncbi.nlm.nih.gov/10649989/.

[9] Yasuhide Ohno, Kenzo Maehashi, and Kazuhiko Matsumoto. "Chemical and biological sensing applications based on graphene field-effect transistors". In: *Biosensors and Bioelectronics* 26.4 (Dec. 2010), pp. 1727–1730. ISSN: 0956-5663. DOI: 10.1016/J.BIOS.2010.08.001.

[10] S.M. Sze and Kwok K. Ng. "Physics of Semiconductor Devices". In: *Physics of Semiconductor Devices* (Oct. 2006). DOI: 10.1002/0470068329. URL: https://onlinelibrary.wiley.com/doi/book/10.1002/0470068329.

[11] H. Y. Zheng and N. O.V. Plank. "Facile fabrication of carbon nanotube network thin film transistors for device platforms". In: *International Journal of Nanotechnology* 14.1-6 (2017), pp. 505–518. ISSN: 14757435. DOI: 10.1504/IJNT.2017.082473.

[12] Yongki Choi, Issa S. Moody, Patrick C. Sims, et al. "Single-molecule lysozyme dynamics monitored by an electronic circuit". In: *Science* 335.6066 (Jan. 2012), pp. 319–324. ISSN: 10959203. DOI: 10.1126/SCIENCE.1214824.

[13] Iddo Heller, Jaan Mãnnik, Serge G. Lemay, et al. "Optimizing the signal-to-noise ratio for biosensing with carbon nanotube transistors". In: *Nano Letters* 9.1 (Jan. 2009), pp. 377–382. ISSN: 15306984. DOI: 10.1021/NL8031636. URL: https://pubs.acs.org/doi/full/10.1021/nl8031636.

[14] Sumio Iijima. "Helical microtubules of graphitic carbon". In: *Nature 1991 354:6348* 354.6348 (1991), pp. 56–58. ISSN: 1476-4687. DOI: 10.1038/354056a0. URL: https://www.nature.com/articles/354056a0.

[15] Han Yue Zheng, Omar A. Alsager, Bicheng Zhu, et al. "Electrostatic gating in carbon nanotube aptasensors". In: *Nanoscale* 8.28 (July 2016), pp. 13659–13668. ISSN: 20403372. DOI: 10.1039/c5nr08117c. URL: https://pubs.rsc.org/en/content/articlehtml/2016/nr/c5nr08117c%20https://pubs.rsc.org/en/content/articlelanding/2016/nr/c5nr08117c.

[16] Thanihaichelvan Murugathas, Cyril Hamiaux, Damon Colbert, et al. "Evaluating insect odorant receptor display formats for biosensing using graphene field effect transistors". In: *ACS Applied Electronic Materials* 2.11 (Nov. 2020), pp. 3610–3617. ISSN: 26376113. DOI: 10.1021/ACSAELM.0C00677. URL: https://pubs.acs.org/doi/full/10.1021/acsaelm.0c00677.

[17] Yann Battie, Olivier Ducloux, Philippe Thobois, et al. "Evaluation of sorted semiconducting carbon nanotube films for gas sensing applications". In: *Comptes Rendus Physique* 11.5-6 (June 2010), pp. 397–404. ISSN: 1631-0705. DOI: 10.1016/J.CRHY.2010.06.004.

[18] Anthony Boyd, Isha Dube, Georgy Fedorov, et al. “Gas sensing mechanism of carbon nanotubes: From single tubes to high-density networks”. In: *Carbon* 69 (Apr. 2014), pp. 417–423. ISSN: 0008-6223. DOI: 10.1016/J.CARBON.2013.12.044.

[19] Jialuo Chen, Ardalan Lotfi, Peter J. Hesketh, et al. “Carbon nanotube thin-film-transistors for gas identification”. In: *Sensors and Actuators B: Chemical* 281 (Feb. 2019), pp. 1080–1087. ISSN: 0925-4005. DOI: 10.1016/J.SNB.2018.10.035.